Int. J. Heat Mass Transfer. Vol. 35, No. 7, pp. 1695–1710, 1992
Printed in Great Britain

0017–9310/92 $5.00 + 0.00

A study of thermal convection in an enclosure induced simultaneously by gravity and vibration

WU SHUNG FU and WEN JIANN SHIEH
Department of Mechanical Engineering, National Chiao Tung University, Hsinchu 30050, Taiwan, Republic of China

(*Received* 1 *February* 1991 *and in final form* 8 *July* 1991)

Abstract—Thermal convection in a two-dimensional square enclosure induced simultaneously by gravity and vertical vibration is investigated numerically. A penalty finite element method with a Newton–Raphson iteration algorithm and a backward difference scheme dealing with the time term are adopted to solve the governing equations. In order to investigate the effects of the vibration frequency and Rayleigh number on the thermal convection in the enclosure, the vibration frequency is varied from 1 to 10^4 and three different values of the Rayleigh number of 0, 10^4 and 10^6 are considered. According to the results, the thermal convection can be divided into five regions: (i) quasi-static convection; (ii) vibration convection; (iii) resonant vibration convection; (iv) intermediate convection; and (v) high frequency vibration convection. In the high Rayleigh number ($=10^6$) case, the gravitational thermal convection dominates, and the vibration motion does not enhance the heat transfer rate remarkably. In contrast, in the low Rayleigh number ($=10^4$) case, except in the quasi-static convection region, the vibration thermal convection is dominant, and the vibration enhances the heat transfer rate significantly. In addition, two analytic methods are proposed to predict the frequencies of the quasi-static convection and resonant vibration convection regions, respectively. The values predicted by the two methods are in agreement with that obtained from the numerical method.

INTRODUCTION

THE STUDY of natural convection in an enclosure has been investigated for decades due to its extensive applications in engineering, like solar energy systems, electronic cooling equipment, crystal growth processes, etc. However, most of the studies have concentrated on the static case, in which the enclosure is fixed on an inertial frame and subjected to a constant gravity only. These kinds of problems have been reviewed extensively by Ostrach [1–3], Catton [4] and Yang [5]. However, there are many practical problems of natural convection in an enclosure occurring in the non-inertial frame which are caused by non-periodic (accelerating–decelerating) or periodic (harmonic vibration) motion. These kinds of problems are rather complicated and difficult; besides, theoretical, numerical or experimental investigations on such problems are comparatively few.

In the past, Richardson [6] reviewed the effects of sound and wall vibration on heat transfer. Gershuni and Zhukhovitsky [7] surveyed the studies of vibrational convection under a zero gravity condition. Forbes *et al.* [8] conducted experiments to investigate the enhancement of thermal convection heat transfer in a liquid-filled rectangular enclosure by vibration; the results showed that the vibration frequency and acceleration were the dominant factors which affected heat transfer, and the effects of vibration amplitude and average velocity were minor. When the vibration frequency was close to the resonant frequency of the liquid column in the enclosure, the heat transfer rate increased very markedly and the value of enhancement was raised by almost 50% compared to the condition under no vibration. In the experimental study, Ivanova and Kozlov [9] considered vibration effects on the natural convection in a horizontal cylinder layer. According to the vibration intensity and the flow type, the flow field was divided into three regimes. In the first regime, laminar motion existed and the enhancement of heat transfer rate was minor, and in the second regime the development of a wave instability in the ascending flow near the heated cylinder was observed and the heat transfer character was similar to the first regime. In the third regime, the threshold development of the vibrational vortices occurred and the increase of heat transfer rate was remarkable. Ivanova [10] studied the vibration effect on the cooling process of the fluid layer between the concentric cylinders. When the wall temperature decreased abruptly, the results showed that increasing the vibration frequency decreased the cooling time of the fluid. Zavarykin *et al.* [11, 12] vibrated the fluid layer vertically or in parallel to its temperature gradient to investigate the effects of vibration on the stability of a hydrodynamic system. The results were in good agreement with the theory. As for the theoretical studies of the related subject, Gershuni and Zhukhovitskii [13] studied the stability of a horizontal layer of fluid on a plane with a periodically varying temperature gradient. They showed that the system could be described by the Hill equation with damping. Subsequently, the study was extended to the modulation of the vertical temperature gradient and the

NOMENCLATURE

b	vibration amplitude [m]
C_p	specific heat [J kg^{-1} K^{-1}]
g	broadest definition of the gravity, $g_0+b\Omega^2 \sin \Omega t$ [m s^{-2}]
g_0	standard gravitational acceleration, 9.8 m s^{-2}
G	vibration Grashof number, $(\beta b\Omega(T_h-T_c)L)^2/2\nu^2$
k	thermal conductivity [W m^{-1} K^{-1}]
L	length of the enclosure [m]
Nu	Nusselt number
$\overline{Nu}$	average Nusselt number
Nu_x	total Nusselt number
$Nu_{x,y}$	local Nusselt number
p	pressure [Pa]
p^*	motion pressure [Pa]
P	dimensionless pressure
Pr	Prandtl number, ν/α
Ra	Rayleigh number, $g_0\beta(T_h-T_c)L^3/(\alpha\nu)$
$Ra(\tau)$	time-dependent Rayleigh number, $g(t)\beta(T_h-T_c)L^3/(\alpha\nu)$
t	time [s]
T	temperature [K]
u, v	velocities of x and y directions [m s^{-1}]
U, V	dimensionless velocities of x and y directions
V^*	velocity scale of the resonant flow
x, y	coordinates
X, Y	dimensionless coordinates.

Greek symbols

α	thermal diffusivity [m^2 s^{-1}]
β	thermal expansion coefficient [K^{-1}]
Γ	period of vibration, $2\pi/\Omega$ [s]
δ_s	thickness of Stokes layer, $4.5\sqrt{(2\nu/\Omega)}$ [m]
θ	dimensionless temperature
μ	viscosity [kg m^{-1} s^{-1}]
ν	kinematic viscosity [m^2 s^{-1}]
ρ	density [kg m^{-2}]
τ	dimensionless time
Ψ	dimensionless stream function
$\Psi_{\max(\text{or min})}$	maximum (or minimum) value of Ψ at a given instant state
$\Psi_{\max(\text{or min}),\max(\text{or min})}$	maximum (or minimum) value of the time history of $\Psi_{\max(\text{or min})}$ in a flow period
ω	dimensionless frequency of vibration, $\Omega L^2/\alpha$
Ω	angular frequency of vibration [rad s^{-1}].

Subscripts

c	cold wall
h	hot wall
r	resonant flow state.

Superscript

m	iteration number.

gravity, and they examined the destabilizing and stabilizing effect of parameter modulation on the convection [14]. Zenkovskaya and Simonenko [15] used the time-averaged method to investigate the stability of fluid flow for high frequency vibration. Later, Gershuni *et al.* [16], Sharifulin [17] and Siraev [18] used the above-mentioned method to study the vibrational thermal convection under the weightlessness condition in a rectangular, cylindrical enclosure and a heated cylinder in an unconfined fluid, respectively. Due to the high frequency assumption, many important phenomena, like the resonant state and the detailed variation of the heat transfer rate, cannot be investigated by solving time-averaged governing equations. However, Yurkov [19, 20] directly solved the Boussinesq-approximated governing equations to investigate the thermal convection in a square enclosure induced by finite-frequency vibration under the weightlessness condition. From the results of the average Nusselt number, the parametric resonant phenomenon was found. Biringen and Danabasoglu [21] studied the effects of gravity modulation in a thermally driven rectangular enclosure for terrestrial and microgravity environments; the results showed that the destabilizing and stabilizing effects of gravity modulation agreed with the theories of Gresho and Sani [22]. Biringen and Peltier [23] studied the three-dimensional Bernard convection with gravitational modulation and confirmed the synchronous, subharmonic and relaxation oscillation response regimes described by the linear analysis of Gresho and Sani [22]. Also, Fu and Shieh [24] studied a square enclosure subjected to an accelerating and decelerating process. From the scale and mathematical analyses, the results showed that the heat transfer rate of the vertical wall could be delineated by the quasi-steady state when the Rayleigh number rate of variation $|\mathrm{d}Ra(\tau)/\mathrm{d}\tau|$ was less than the boundary response rate $Pr^{1/2}|Ra(\tau)|^{3/2}$. As for the theoretical study of thermal convection induced by vibration and gravity in an enclosure, few such investigations have been conducted. Thus, knowledge of behavior in this field is important in many practical engineering problems.

Hence, the aim of the study is to investigate numerically the detailed heat transfer mechanism of thermal convection which is induced by gravity and vibration simultaneously in a square enclosure at steady state. A finite element method is used to solve the Boussinesq-approximated governing equations. Since in this case there are many factors that affect the heat transfer

mechanism and the vibration perpendicular to the temperature gradient is the most critical [21], we mainly consider the effects of the vertical vibration frequency on heat transfer mechanism. The range of vibration frequency ω varies from 1 to 10^4, in which the resonant frequency is included. The accompanying factors of Rayleigh number are 0, 10^4 and 10^6, respectively, the vibration Grashof number is fixed at 10^6 and the Prandtl number is 0.71. Corresponding to the variations of vibration frequency from low to high, the flow field and heat transfer rate change from the quasi-static state region via a resonant region to a high frequency region, and in the resonant region the heat transfer rate varies drastically. The streamlines, isothermal lines and the variations of Nusselt number and stream function are also examined in detail.

PHYSICAL MODEL

An air-filled ($Pr = 0.71$) square enclosure with two horizontal adiabatic walls and two vertical constant temperature walls at which the temperature of the left wall is higher than that of the right wall is proposed in this study and a sketched model is shown in Fig. 1. Initially ($t = 0$), the flow in the enclosure is at steady flow state with the corresponding Rayleigh number under the no vibration condition. Later ($t > 0$), the enclosure is subjected to a vertical vibration with the displacement $-b \sin(\Omega t)$ parallel to the direction of gravity. Then a non-inertial frame of reference traveling with the enclosure is used and the parameters b, Ω and t are respectively the displacement amplitude, angular frequency and time.

In order to facilitate the analysis, the following assumptions and dimensionless variables are considered.

1. The fluid is Newtonian and the flow is two-dimensional laminar.
2. The vibration velocity amplitude $b\Omega$ is not large and the flow is assumed to be incompressible [25].
3. The Boussinesq approximation is valid.

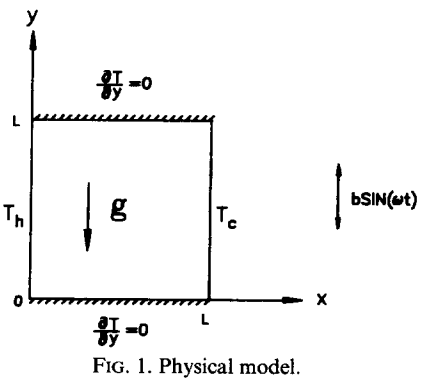

FIG. 1. Physical model.

$$\tau = t/(L^2/\alpha), \quad X = x/L, \quad Y = y/L,$$

$$U = u/(\alpha/L), \quad V = v(\alpha/L), \quad \theta = (T-T_c)/(T_h-T_c),$$

$$P = p^*/(\rho_c\alpha^2/L^2), \quad \omega = \Omega L^2/\alpha, \quad Pr = \nu/\alpha,$$

$$Ra = g_0\beta(T_h-T_c)L^3/(\alpha\nu),$$

$$G = (\beta b\Omega(T_h-T_c)L)^2/2\nu^2, \tag{1}$$

in which G is called the vibration Grashof number [7].

Consequently, the dimensionless governing equations can be expressed as follows:

$$\frac{\partial U}{\partial X} + \frac{\partial V}{\partial Y} = 0 \tag{2a}$$

$$\frac{\partial U}{\partial \tau} + U\frac{\partial U}{\partial X} + V\frac{\partial U}{\partial Y} = -\frac{\partial P}{\partial X} + Pr\left(\frac{\partial^2 U}{\partial X^2} + \frac{\partial^2 U}{\partial Y^2}\right) \tag{2b}$$

$$\frac{\partial V}{\partial \tau} + U\frac{\partial V}{\partial X} + V\frac{\partial V}{\partial Y} = -\frac{\partial P}{\partial Y} + Pr\left(\frac{\partial^2 V}{\partial X^2} + \frac{\partial^2 V}{\partial Y^2}\right) + Pr(Ra + \omega\sqrt{(2G)}\sin\omega\tau)\theta \tag{2c}$$

$$\frac{\partial \theta}{\partial \tau} + U\frac{\partial \theta}{\partial X} + V\frac{\partial \theta}{\partial Y} = \frac{\partial^2 \theta}{\partial X^2} + \frac{\partial^2 \theta}{\partial Y^2}. \tag{2d}$$

The boundary conditions are as follows:

$$X = 0, \quad U = V = 0, \quad \theta = 1$$

$$X = 1, \quad U = V = \theta = 0$$

$$Y = 0 \quad \text{and} \quad Y = 1, \quad U = V = \partial\theta/\partial Y = 0. \tag{3}$$

SOLUTION METHOD

The penalty Galerkin finite element method with a Newton–Raphson algorithm and a backward difference scheme dealing with the time term which is similar to the one used in Fu *et al.* [26] are employed to solve the governing equations (2a)–(2d). A nine-node quadratic isoparametric element is used to express the velocities and temperature terms which are integrated by 3×3 Gaussian quadrature, while the pressure term is expressed by the penalty function and integrated by 2×2 Gaussian quadrature. During the computing process, the convergent values of velocities and temperature of the lower frequency vibration situation are used as the initial values for the neighboring high frequency vibration cases. The velocities and temperature at steady flow state with the corresponding Rayleigh number under no vibration are regarded as the initial values of the lowest frequency vibration situation. As for the criteria for steady flow state under periodic motion, it is difficult to define them definitely. Then, except in the resonant region, while the following criteria are satisfied the flow is regarded as reaching the steady flow state:

$$\left|\frac{\phi^{m+1}-\phi^{m}}{\phi^{m+1}}\right| < 10^{-3}, \quad \phi = U, V \text{ and } \theta \qquad (4a)$$

and

$$\left|\frac{Nu_{L,n+1}-Nu_{L,n}}{Nu_{L,n+1}}\right| < 10^{-3} \quad n = k-3, \ldots, k. \qquad (4b)$$

$Nu_{L,n}$ represents the nth extremum (maximum and minimum) of the left wall Nusselt number in the time history. Equation (4b) indicates that the relative variations of four successive extrema of the left wall Nusselt number are less than 10^{-3}. When the above criteria hold, the difference of energy balance of the enclosure is always less than 10^{-5} and the error of mass conservation is always less than 10^{-7}.

The local Nusselt number $Nu_{x,y}$ on any vertical plane is defined as

$$Nu_{x,y} = \left[\rho C_p u(T-T_c) - k\frac{\partial T}{\partial x}\right] \Big/ [k(T_h-T_c)/L]. \qquad (5)$$

The total Nusselt number Nu_x on any vertical plane is defined as

$$Nu_x = \int_0^1 Nu_{x,y}\,dY. \qquad (6)$$

The dimensionless stream function Ψ is obtained by integrating $U = \partial\Psi/\partial Y$ with $\Psi = 0$ along the walls.

For choosing the proper mesh and time step during the computation process, a series of numerical tests is carried out. The results for $Ra = 10^4$, $G = 10^6$, $\omega = 810$ (case I) and $Ra = 10^6$, $G = 10^6$, $\omega = 800$ (case II) are presented. First, the meshes are tested with the static case (without vibration) and the results are compared with those of De Vahl Davis [27] in Table 1. This shows that the accuracy of the mesh 10×10 elements and 13×13 elements are valid for the $Ra = 10^4$ and $Ra = 10^6$ cases, respectively. Next, the cases with vibration are considered and the results are shown in Fig. 2. In the figure, the characters Max, Avg and Min represent, respectively, the maximum, time-averaged and minimum values of the different variables. The time-averaged value is calculated by

$$\frac{1}{t_2-t_1}\int_{t_1}^{t_2}\phi(t)\,dt \qquad (7)$$

in which t_1 and t_2 represent the times of the neighboring extrema after reaching steady flow state. The Simpson one-third method is employed to integrate equation (7) numerically. The NCYCLE in the figures indicates the number of time intervals per vibrational period $(2\pi/\omega)$ used in the computation. For counting the peak of the vibrational force $\omega\sqrt{(2G)}\sin\omega\tau$ exactly in the computation, the NCYCLE must be a multiple of 4. The results of the extrema of the Nusselt number and the minimum stream function with different meshes of 10×10, 13×13, 16×16 and 18×18, respectively, are shown in Figs. 2(a) and (b). From the results, the mesh 10×10 elements and 13×13 elements are found to be valid for the above two vibrational cases, respectively. The results of the different NCYCLEs with a 10×10 element mesh for case I and a 13×13 element mesh for case II are shown

Table 1. Comparisons of the results of the present study with De Vahl Davis [27]

	$Ra = 10^4$				$Ra = 10^6$				
	Bench-mark solution	De Vahl Davis 41×41 uniform	Authors 13×13 elements	Authors 10×10 elements	Bench-mark solution	De Vahl Davis 61×61 uniform	Authors 16×16 elements	Authors 13×13 elements	Authors 10×10 elements
$\lvert\Psi_{mid}\rvert$	5.071	5.098 (0.53%)	5.075 (0.079%)	5.074 (0.059%)	16.32	16.67 (2.14%)	16.395 (0.46%)	16.40 (0.49%)	16.40 (0.49%)
$U_{max,x=0.5}$	16.178	16.182 (0.025%)	16.106 (0.44%)	16.095 (0.51%)	64.63	65.81 (1.82%)	64.789 (0.24%)	64.28 (0.54%)	64.24 (0.60%)
Y	0.823	0.823	0.838	0.839	0.850	0.852	0.854	0.838	0.839
$V_{max,y=0.5}$	19.617	19.509 (0.55%)	19.526 (0.46%)	19.621 (0.02%)	219.36	214.64 (2.15%)	219.39 (0.01%)	220.17 (0.37%)	220.98 (0.70%)
X	0.119	0.120	0.108	0.125	0.0379	0.0396	0.04167	0.0405	0.0357
$\overline{Nu}$	2.243	2.234 (0.40%)	2.254 (0.49%)	2.259 (0.71%)	8.800	8.794 (0.07%)	8.851 (0.57%)	8.855 (0.62%)	8.926 (1.43%)
$Nu_{x=0.5}$	2.243	2.235 (0.36%)	2.266 (1.02%)	2.274 (1.38%)	8.799	8.823 (0.07%)	8.818 (0.21%)	8.817 (0.20%)	8.832 (0.37%)
$Nu_{x=0}$	2.238	2.242 (0.18%)	2.246 (0.36%)	2.248 (0.45%)	8.817	9.035 (2.47%)	8.935 (1.32%)	9.036 (2.48%)	9.230 (4.68%)
$Nu_{max,x=0}$	3.528	3.545 (0.48%)	3.529 (0.028%)	3.531 (0.085%)	17.925	18.255 (1.84%)	17.930 (0.03%)	18.207 (1.57%)	18.600 (3.76%)
Y	0.143	0.149	0.162	0.161	0.0378	(0.0523)	0.04167	0.0441	(0.0357)
$Nu_{min,x=0}$	0.586	0.592 (1.02%)	0.586 (0.0%)	0.587 (0.17%)	0.989	1.002 (1.31%)	0.987 (0.2%)	0.988 (0.10%)	1.013 (2.43%)
Y	1.0	1.0	1.0	1.0	1.0	1.0	1.0	1.0	1.0

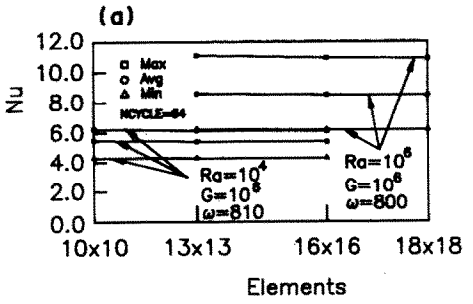

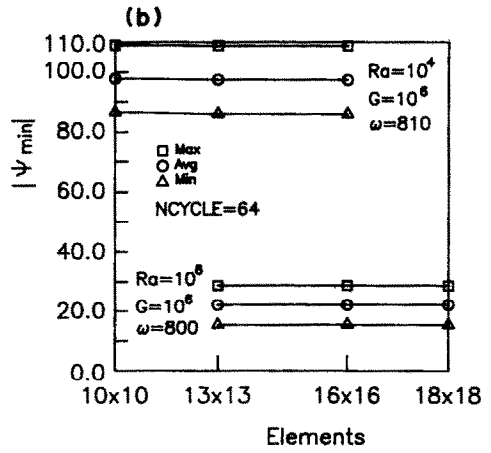

FIG. 2. Numerical results for various meshes. (a) Nusselt numbers. (b) The minimum values of stream function.

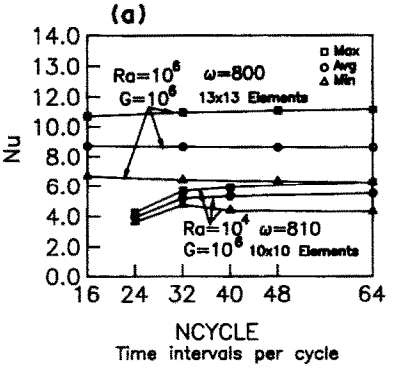

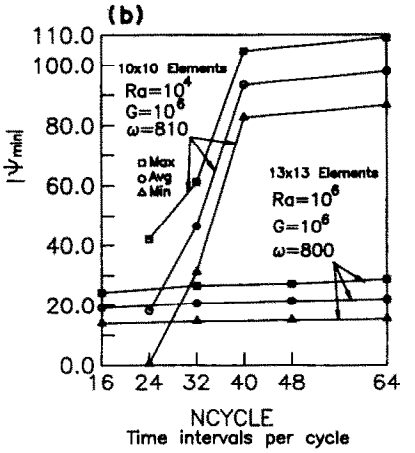

FIG. 3. Numerical results for various time steps. (a) Nusselt numbers. (b) The minimum values of stream function.

in Fig. 3. The results show clearly that NCYCLE = 64 and NCYCLE = 48 are, respectively, enough for solving the problems of cases I and II accurately.

RESULTS AND DISCUSSION

In Fig. 4, the variations of the values of the maximum (□), average (○) and minimum (△) of Nu, $|\Psi_{min}|$ and Ψ_{max} with the frequency ω for the case of $Ra = 10^4$, $G = 10^6$ are shown. In Fig. 4(a), the dashed lines which are obtained from the following correlating equation represent the values of the maximum, average and minimum of the total Nusselt numbers of the quasi-static state:

$$Nu = \max(1.0, 0.1388|R|^{0.3025})$$

$$R = Ra + \omega\sqrt{(2G)}\sin\omega\tau. \tag{8}$$

The data used to derive equation (8) are obtained from the total Nusselt number of the left wall at the statically steady state of the Rayleigh numbers of 10^4, 10^5 and 10^6. In Fig. 4(a), the Nusselt numbers are in good agreement with the dashed lines in the range of $\omega < 10$, which means that static convection is dominant and the vibration is regarded as a disturbance added to the fluid flow. This region is called the quasi-static convection region.

According to the results of Fu and Shieh [24], the reason for the total Nusselt number deviating from the dashed lines in this region may be supposed to be due to the response of the thermal boundary layer near the vertical wall which cannot catch up with the variation $Ra(\tau)$. In turn, while the following inequality is determined, the deviation between the total Nusselt number and the dashed line will occur:

$$\left|\frac{dRa(\tau)}{d\tau}\right| > Pr^{1/2}|Ra(\tau)|^{3/2}, \tag{9}$$

in which $Ra(\tau) = Ra + \omega\sqrt{(2G)}\sin\omega\tau$ in this paper. Then

$$\left|\frac{dRa(\tau)}{d\tau}\right| = |\omega^2\sqrt{(2G)}\omega\tau|. \tag{10}$$

In this region, the vibration is regarded as a disturbance to the static convection, and

$$Ra(\tau) \simeq Ra. \tag{11}$$

Substituting equations (10) and (11) into (9), the frequency ω is about 24, which is close to the frequency

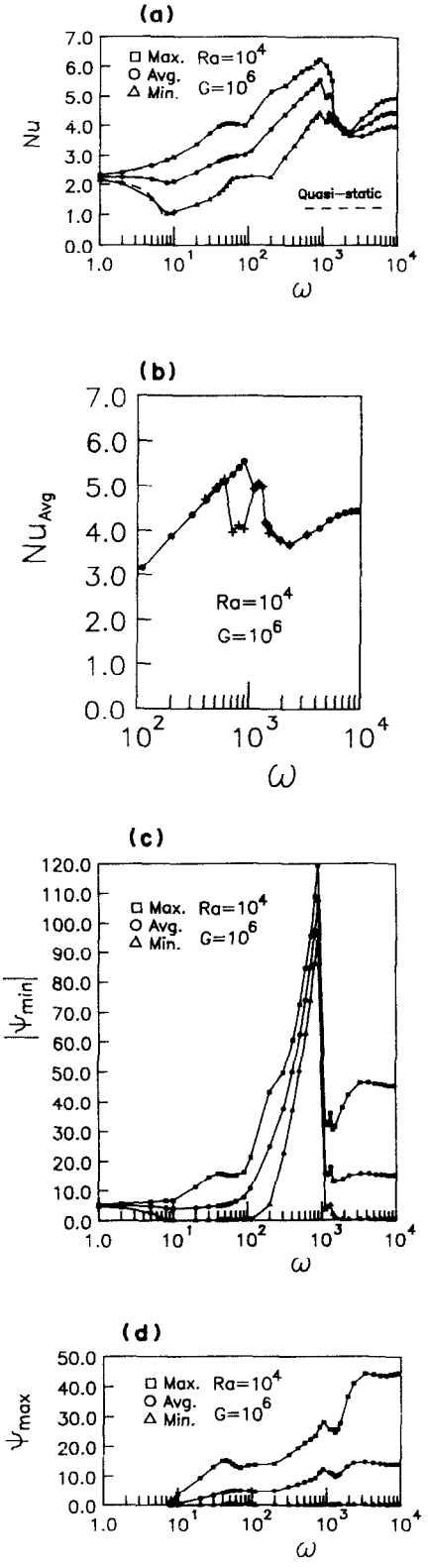

FIG. 4. Effects of the vibration frequency on thermal convection for $Ra = 10^4$, $G = 10^6$. (a) The variations of Nusselt number with the vibration frequency. (b) The jump phenomenon of average Nusselt number. (c) The variations of the minimum value of stream function with the vibration frequency. (d) The variations of the maximum value of stream function with the vibration frequency.

($\simeq 10$) obtained from the numerical result shown in Fig. 4(a).

For $10 \leqslant \omega < 110$, the values of Nusselt number begin to deviate from the values calculated from equation (14) and the former are larger than the latter. Since the Rayleigh number is small, then the vibration affects and enhances the heat transfer rate even in the low frequency range. According to the domination of vibration convection, the counter-clockwise rotating flow (Fig. 4(d)) not only forms, but also has strength of the same order of magnitude as the clockwise rotating flow (Fig. 4(c)). This region is called the vibration convection region.

For $110 \leqslant \omega \leqslant 900$, the resonant vibration phenomenon occurs, which causes the strength of $|\Psi_{min}|$ to increase significantly (Fig. 4(c)) and the heat transfer rate (Fig. 4(a)) to be enhanced remarkably. This region is called the resonant vibration convection region. The increasing rate of Nusselt number in this region is about 2.7 times that in the vibration convection region. The maximum value of $|\Psi_{min}|$ occurs at $\omega = 900$, which is defined as the resonant frequency.

For $900 < \omega \leqslant 2310$, the Nusselt number decreases abruptly, and the intensity of the clockwise cell (Fig. 4(c)) decreases rapidly and approximately equals the intensity of the counter-clockwise rotating cell (Fig. 4(d)). Then the flow pattern changes from the resonant vibration convection region to the high frequency vibration convection region. This region is called the intermediate convection region. In order to examine in detail the drastic variation (jump phenomenon) of the Nusselt number, which occurred in the weightlessness condition [20] and in a damped Duffin's spring [28], at the border between the resonant and high frequency vibration regions, the solutions for $400 \leqslant \omega \leqslant 3310$ are solved by the decreasing frequency process from 3310 to 400 and compared with the previous solutions, which are solved by the increasing frequency process. The results are shown in Fig. 4(b), where open circles (○) represent the solutions obtained by the increasing frequency process and plus signs (+) represent the solutions obtained by the decreasing frequency process. The results show that while $\omega \geqslant 1110$ or $\omega \leqslant 600$, the average Nusselt numbers obtained by both processes are the same. However, for $600 < \omega < 1110$, the average Nusselt number obtained by the increasing frequency process is larger than that obtained by the decreasing frequency process. The solutions obtained by the decreasing frequency process at $\omega = 1210, 1110, 900, 810, 710$ and increasing frequency process at $\omega = 1110, 1210$ are aperiodic.

For $\omega > 2310$, the vibration frequency is high, and the fluid flow becomes a multi-frequency motion, which causes the difference between the maximum and minimum Nusselt numbers to be enlarged again. The values of $|\Psi_{min}|$ (Fig. 4(c)) and Ψ_{max} (Fig. 4(d)) are almost equivalent, which means that the vibration convection is dominant, and contrarily the static

gravitational convection is regarded as a disturbance added to the flow. This region is called the high frequency vibration convection region.

In Fig. 5 the variations of the values of the maximum (□), average (○) and minimum (△) of Nu, $|\Psi_{min}|$ and Ψ_{max} with the frequency ω for the case of $Ra = 10^6$, $G = 10^6$ are shown. The dashed lines are obtained from the correlation, equation (8). The values of the average Nusselt number are consistent with the dashed line in the range of $\omega \leqslant 600$ (Fig. 5(a)); in the meantime the maximum and minimum values of $|\Psi_{min}|$ are symmetric to the average value (Fig. 5(b)), and the value of Ψ_{max} is zero which indicates that the counter-clockwise cell does not exist (Fig. 5(c)). The vibration motion is regarded as a disturbance added to the static convection. This phenomenon is similar to the quasi-static convection region of the case of $Ra = 10^4$, $G = 10^6$ mentioned above.

Calculating equations (9), (10) and (11), mentioned above, the frequency approximately equals 770, which is also close to the frequency ($\simeq 600$) obtained from the numerical result shown in Fig. 5(a).

For $600 < \omega \leqslant 800$, the total Nusselt number starts to deviate from the dashed line. Due to the high Rayleigh number situation, the maximum and minimum values of $|\Psi_{min}|$ are symmetric to the average value of $|\Psi_{min}|$, and the value of Ψ_{max} is near zero. This region is called the vibration convection region.

For $800 < \omega < 3000$, the variations of Nu, $|\Psi_{min}|$ and Ψ_{max} are drastic, and the region is called the resonant vibration convection region. Ψ_{max} appears explicitly in this region, but its value is smaller than that of $|\Psi_{min}|$. For the high Rayleigh number situation, the resonant vibration flow does not increase the Nusselt number very much, like the $Ra = 10^4$, $G = 10^6$ case, and the average Nusselt number is smaller than that of the quasi-static convection region. The maximum value of $|\Psi_{min}|$ occurs at $\omega = 900$, which is defined as the resonant frequency.

For $\omega \geqslant 3000$, the average Nusselt numbers are nearly invariant and the maximum and minimum Nusselt numbers increasingly converge to the average value. Because the Rayleigh number is high, the effect of the high frequency vibration on the heat transfer rate is not significant. The intensity of $|\Psi_{min}|$ is still larger than that of Ψ_{max} due to the strong thermo-gravitational convection. This region is called the high frequency vibration convection region. Since the flow induced by the static convection is strong, the intermediate convection region mentioned for the $Ra = 10^4$, $G = 10^6$ case cannot be found in this case. This is another characteristic of the high Rayleigh number situation.

Shown in Fig. 6 are the variations of the Nusselt number and stream function with the vibration frequency for the $Ra = 0$, $G = 10^6$ case, which means the weightlessness situation. Except for the quasi-static region, the variations of the Nusselt number and stream function are almost consistent with those of the $Ra = 10^4$, $G = 10^6$ case in the whole frequency range. The four regions are: (i) the vibration convection region for $\omega \leqslant 100$; (ii) the resonant vibration convection region, for $100 < \omega \leqslant 900$; (iii) the intermediate region for $900 < \omega \leqslant 2300$; and (iv) the high frequency region for $\omega > 2300$. The behavior of the

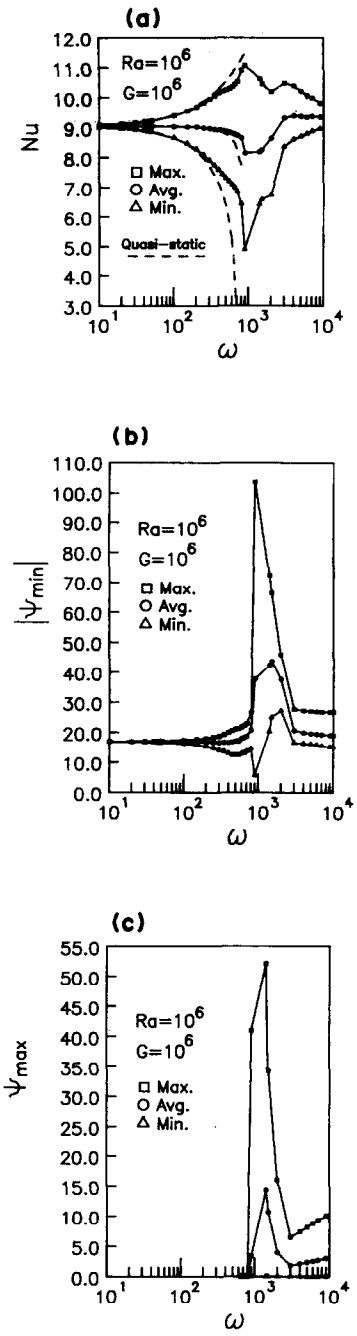

FIG. 5. Effects of the vibration frequency on thermal convection for $Ra = 10^6$, $G = 10^6$. (a) The variations of Nusselt number with the vibration frequency. (b) The variations of the minimum value of stream function with the vibration frequency. (c) The variations of the maximum value of stream function with the vibration frequency.

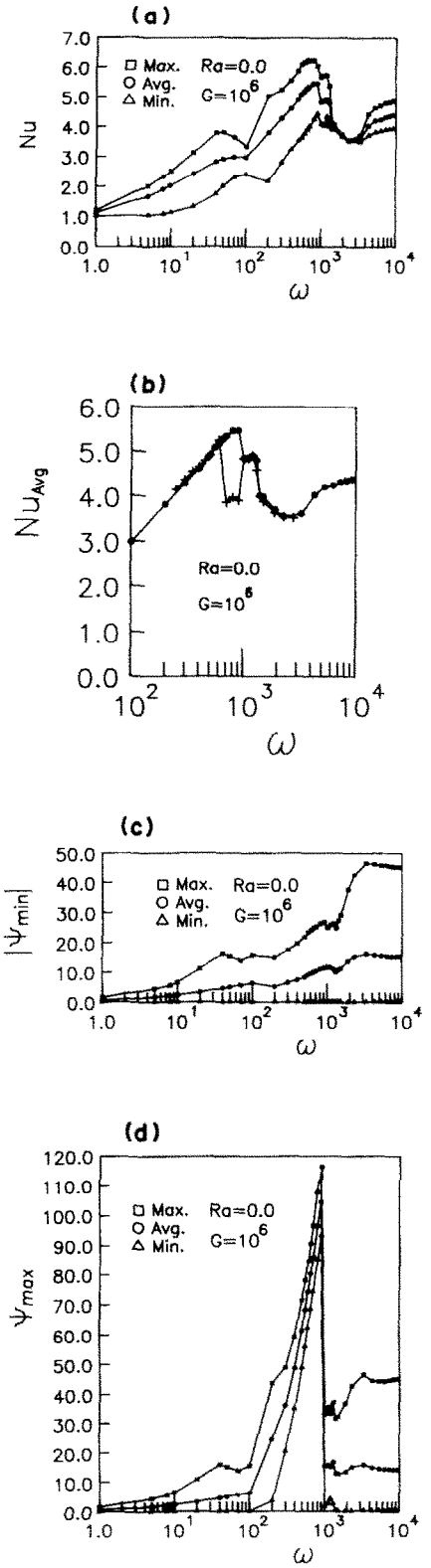

FIG. 6. Effects of the vibration frequency on thermal convection for $Ra = 0$, $G = 10^6$. (a) The variations of Nusselt number with the vibration frequency. (b) The jump phenomenon of average Nusselt number. (c) The variations of the minimum value of stream function with the vibration frequency. (d) The variations of the maximum value of stream function with the vibration frequency.

stream function in the resonant vibration convection region is opposite to that of the $Ra = 10^4$, $G = 10^6$, case, which is caused by the different initial condition in the computation. Similar to the $Ra = 10^4$, $G = 10^6$ case, the jump phenomenon also occurs in this case. The solutions obtained by the increasing (circle ○) and decreasing (plus +) frequency processes are shown in Fig. 6(b), and are similar to those of Fig. 4(b).

The isotherms and streamlines of case I ($Ra = 10^4$, $G = 10^6$) with the vibration frequencies 110, 900, 1510 and 5310 are, respectively, shown in Figs. 7–10. In Fig. 7, the thermo-gravitational convection is weak due to the low Rayleigh number; therefore the effect of vibration on the fluid flow is remarkable even for the low frequency ($\omega = 110$) situation. As a result, the cells with opposite rotating directions are co-existent and the regions of the isotherms not only gather densely near the lower and higher regions of the left and right vertical walls (Fig. 7(b)), respectively, but also the entirely opposite regions at a certain phase (Fig. 7(d)).

In Fig. 8, $\omega = 900$ is in the resonant vibration range. The isotherms gather densely near the vertical walls and the fluid flows mainly in the clockwise direction

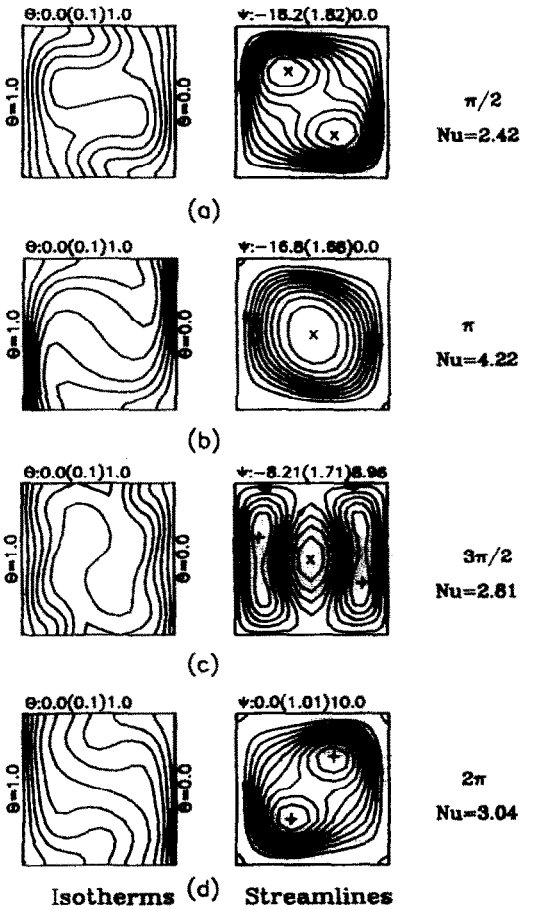

FIG. 7. Isotherms and streamlines for $Ra = 10^4$, $G = 10^6$, $\omega = 110$. (a) $\alpha = 2\pi/2$, (b) $\alpha = \pi$, (c) $\alpha = 3\pi/2$, (d) $\alpha = 2\pi$.

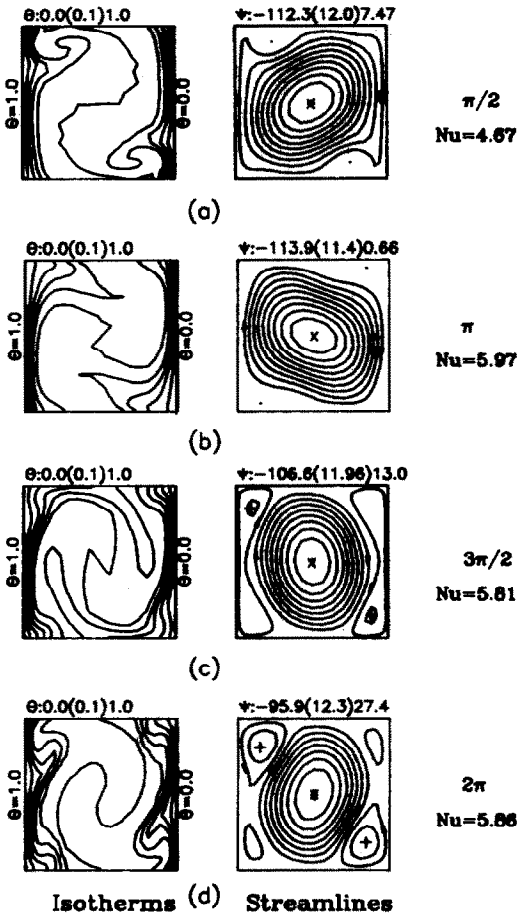

FIG. 8. Isotherms and streamlines for $Ra = 10^4$, $G = 10^6$, $\omega = 900$. (a) $\alpha = \pi/2$, (b) $\alpha = \pi$, (c) $\alpha = 3\pi/2$, (d) $\alpha = 2\pi$.

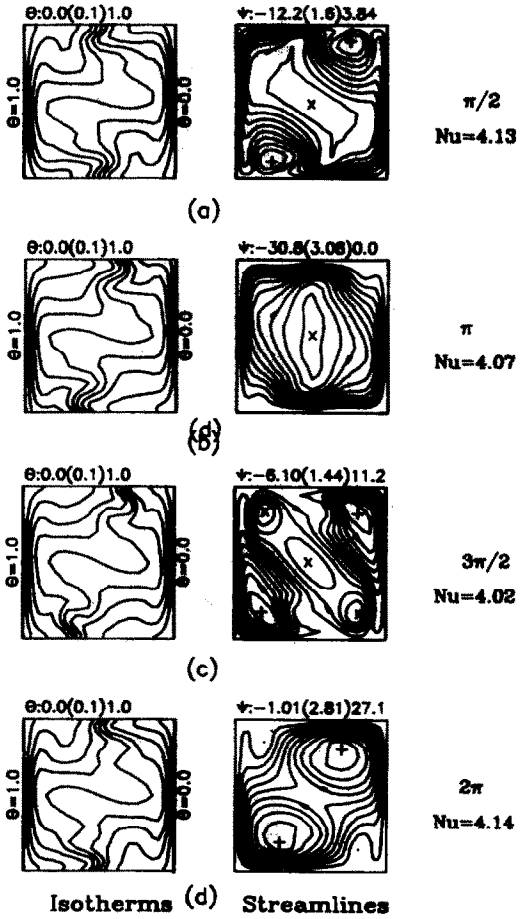

FIG. 9. Isotherms and streamlines for $Ra = 10^4$, $G = 10^6$, $\omega = 1510$. (a) $\alpha = \pi/2$, (b) $\alpha = \pi$, (c) $\alpha = 3\pi/2$, (d) $\alpha = 2\pi$.

like a rotating flow around the core region. The conclusion can be drawn from the results that while the resonant phenomenon occurs, the vibration motion plays the dominant role and the influence of thermo-gravitational convection is negligible. Consequently, the total Nusselt number is constantly much larger than that of static convection ($Nu = 2.24$ for $Ra = 10^4$ [26]) during the whole period.

In Fig. 9, the vibration frequency ω equals 1510. The intensities of the counter-clockwise and clockwise cells have almost the same order and the difference in the total Nusselt number at every different phase is small. The distributions of isotherms shown in the figures are similar, and the regions of the isotherms gathering densely are in the middle region of the vertical walls.

In Fig. 10, the vibration frequency ω equals 5310. The period of fluid flow is 12 times the vibration period (from Fig. 15(e)). Since the variations of isotherms and streamlines are qualitatively similar in every vibration period, the results of the one vibration period are shown in the figures. According to the high frequency ω, the tendency of the clockwise and counter-clockwise cells forming individually is more apparent than that of the low frequency situation.

Figures 11–14, for case II ($Ra = 10^6$, $G = 10^6$) with frequencies of $\omega = 200$, 800, 1500 and 9000, respectively, indicate the distributions of the isotherms and streamlines of a period of fluid flow which includes one or several periods of vibration motion.

In Fig. 11, due to the situation of high Rayleigh number ($Ra = 10^6$) and low frequency ($\omega = 200$), thermo-gravitational convection is dominant, which causes the variations of streamlines and isotherms to be minute with respect to static convection [26]. In Fig. 12, the vibration frequency ω is 800 and is near to the resonant frequency, so the effect on the fluid flow becomes increasingly apparent and the variations of the streamlines and isotherms are rather different from those of static convection. Accompanying the vibration motion, the intensity of the stream function varies periodically and the isotherms in the core region swing to and fro. Because the development of fluid flow lags to the vibration motion, the largest and smallest Nusselt numbers no longer occur near the phases of $\pi/2$ and $3\pi/2$, respectively. This phenomenon is similar to that of natural convection in an enclosure under the time-dependent acceleration situation [24]. Besides, the positive values of the stream function begin to appear but the values are negligibly small. In

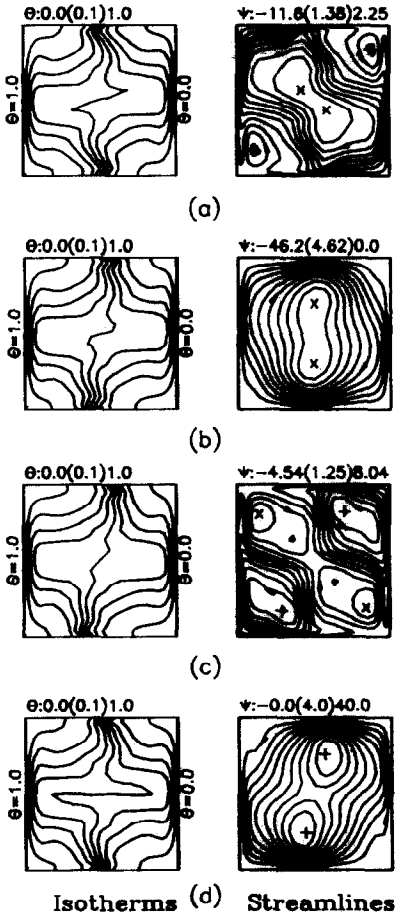

FIG. 10. Isotherms and streamlines for $Ra = 10^4$, $G = 10^6$, $\omega = 5310$. (a) $\alpha = \pi/2$, (b) $\alpha = \pi$, (c) $\alpha = 3\pi/2$, (d) $\alpha = 2\pi$.

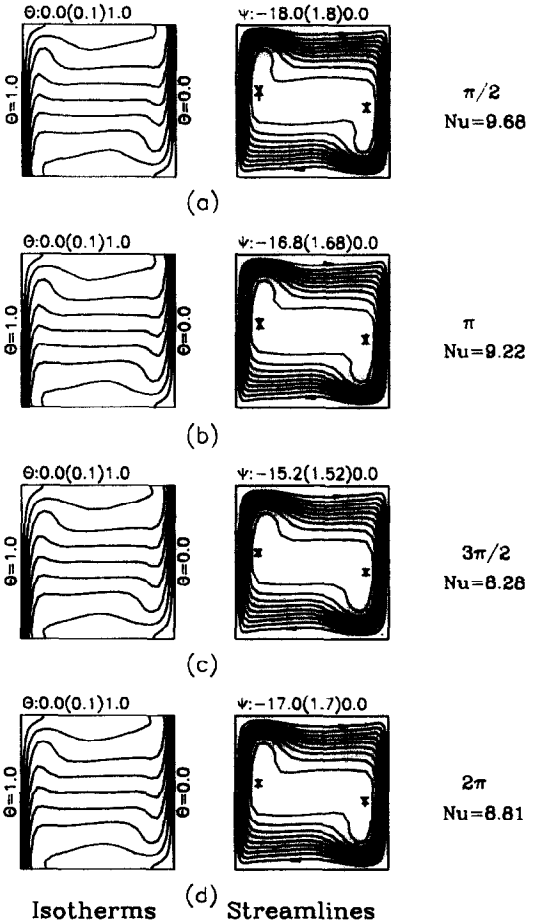

FIG. 11. Isotherms and streamlines for $Ra = 10^6$, $G = 10^6$, $\omega = 200$. (a) $\alpha = \pi/2$, (b) $\alpha = \pi$, (c) $\alpha = 3\pi/2$, (d) $\alpha = 2\pi$.

Fig. 13, the vibration frequency ω is enlarged to 1500, which is in the resonant range. In the figures, two consecutive vibration periods are combined as a period of the fluid flow. The first period is from Figs. 13(a) to (b) and the second period is from Figs. 13(c) to (d). The effect of vibration on the fluid flow is more remarkable than the former situations. The isotherms swing to and fro drastically, and some of them form closed regions (Figs. 13(b) and (c)). The value of $|\Psi_{min}|$ (Fig. 13(c), $|\Psi_{min}| = 66.3$) is greater than that of static convection by several times ($|\Psi_{min}| = 16.7$ [26]). Furthermore, the velocity boundary layer no longer exists, and the fluid flows nearly uniformly around the enclosure (Fig. 13(c)).

When the vibration frequency ω is raised to 9000, the results shown in Fig. 14 are similar to those of the static case [26]. The cause is considered to be that the period of high frequency vibration is too short; in turn the variation between enhancing and weakening buoyancy force is too short, which causes the fluid flow to be unable to catch up with the variation. Consequently, the effect of high frequency vibration on the fluid flow is like a disturbance which somewhat enhances thermo-gravitational convection added to the fluid flow.

Since the Rayleigh number ($Ra = 10^6$) is high, which causes thermo-gravitational convection to be strong, then the isotherms constantly gather densely near the lower region of the left wall and the higher region of the right wall during the variation of vibration frequency from low to high.

The variations of the Nusselt number and stream function with the phase angle α are shown in Figs. 15 and 16 for case I ($Ra = 10^4$, $G = 10^6$) and case II ($Ra = 10^6$, $G = 10^6$), respectively. In Fig. 15(a), the region ($\omega = 110$) is in the vibration convection region, and the phase shift between the maximum values of Ψ_{max} and $|\Psi_{min}|$ is nearly π. The values of Ψ_{max} and Ψ_{min} appear alternatively. In Fig. 15(b), $\omega = 900$ is in the resonant vibration convection region. The clockwise rotating flow (Ψ_{min}) is much stronger than the counter-clockwise rotating flow (Ψ_{max}). The phase shift between the maximum values of Nu and $|\Psi_{min}|$ approximately equals $\pi/2$. As the frequency increases up to 1110 (Fig. 15(c)), the Nusselt number and stream function vary irregularly. The results cannot be improved even if the mesh and time step are increased massively. The exact periodic solutions are hardly found in spite of calculating hundreds of vibration periods. The results shown in the figure are com-

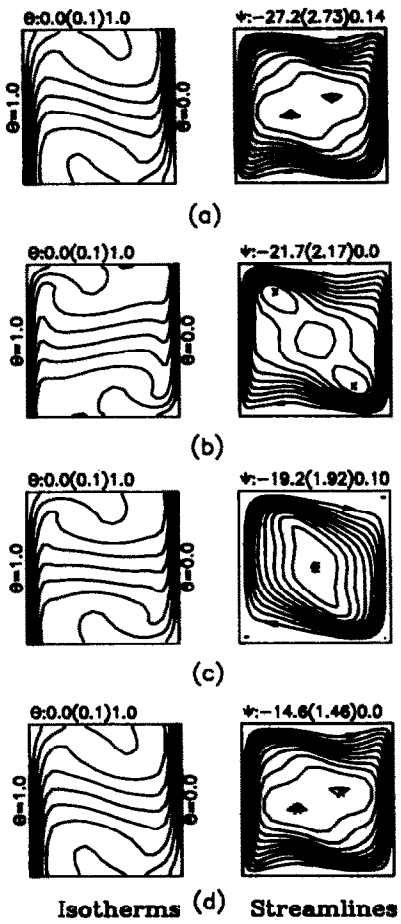

FIG. 12. Isotherms and streamlines for $Ra = 10^6$, $G = 10^6$, $\omega = 800$. (a) $\alpha = \pi/2$, (b) $\alpha = \pi$, (c) $\alpha = 3\pi/2$, (d) $\alpha = 2\pi$.

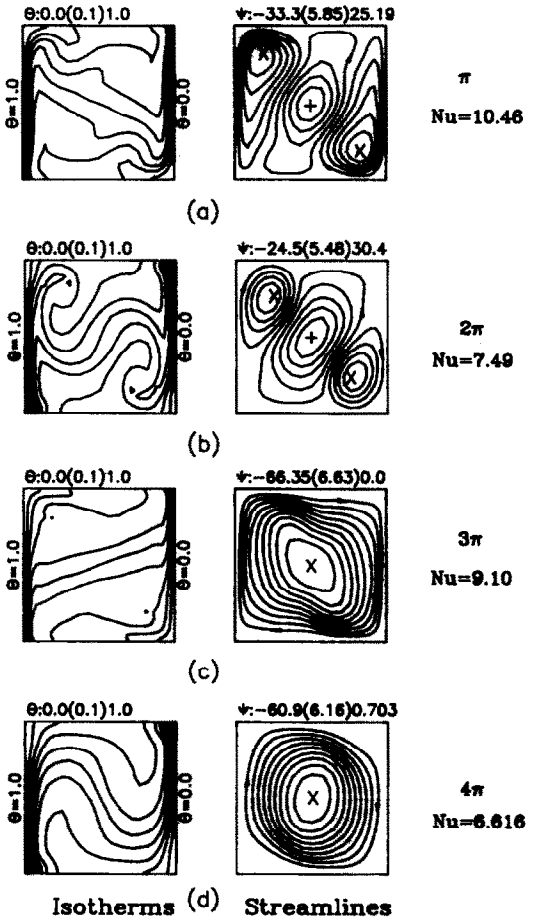

FIG. 13. Isotherms and streamlines for $Ra = 10^6$, $G = 10^6$, $\omega = 1500$. (a) $\alpha = \pi$, (b) $\alpha = 2\pi$, (c) $\alpha = 3\pi$, (d) $\alpha = 4\pi$.

paratively periodic ones. The data used in equation (13) are about 16 periods. The results of $\omega = 1210$ in this case are also irregular and similar to Fig. 15(c). In Fig. 15(d), $\omega = 1510$, which is in the intermediate region, and the difference between the maximum and minimum Nusselt number is smaller than 5%; the phase shift between the maximum values of Ψ_{max} and $|\Psi_{min}|$ equals π. In Fig. 15(e), ω equals 5310, which is in the high frequency vibration convection region. A multi-frequency response occurs, and a flow period consists of approximately 12 vibration periods. It is noted that the variation of the Nusselt number is small in every vibration period, but is large in one flow period. This phenomenon occurs when the frequency is larger than 3310.

Figure 16 shows the variations of the Nusselt number and stream function with the vibration phase angle α for case II ($Ra = 10^6$, $G = 10^6$). In Fig. 16(a), in the region of quasi-static convection ($\omega = 200$), the Nusselt number and flow intensity ($|\Psi_{min}|$) vary nearly in-phase with the vibration. In Fig. 16(b), $\omega = 800$, since the variation of the thermal boundary layer lags the vibration motion, and the maximum Nusselt number does not occur at the maximum value of the stream function. In Fig. 16(c), the frequency ω (=900) is in the resonant vibration region. The flow varies irregularly even if the mesh and time step are increased massively. This phenomenon is similar to that of Fig. 15(c). In Fig. 16(d), the frequency ω (=1500) is still in the resonant vibration region, the period of the flow is twice that of the vibration period and the phase shift between the maximum Nusselt number and the vibration is nearly $\pi/2$. In Fig. 16(e), $\omega = 9000$, which is in the high frequency vibration region, the phase shift between the maximum Nusselt number and the vibration approaches π, and Ψ_{max} and Ψ_{min} are out-of-phase with π.

THE PRELIMINARY ESTIMATION FOR THE RESONANT VIBRATION FREQUENCY

In the resonant vibration convection region ($\omega_r \approx 900$ for $Ra = 10^4$, $G = 10^6$ and $\omega_r \approx 900$ for $Ra = 10^6$, $G = 10^6$), there is no velocity boundary layer, instead of the fluid flowing nearly uniformly around the enclosure, the main rotating direction is almost invariant. As for the isotherms, near both vertical walls the isotherms gather densely and are par-

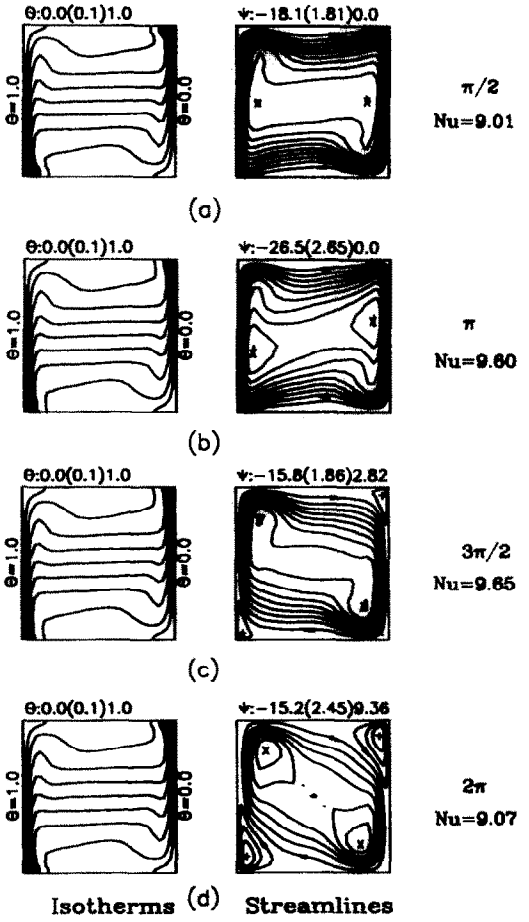

FIG. 14. Isotherms and streamlines for $Ra = 10^6$, $G = 10^6$, $\omega = 9000$. (a) $\alpha = \pi/2$, (b) $\alpha = \pi$, (c) $\alpha = 3\pi/2$, (d) $\alpha = 2\pi$.

allel to the walls, in the core region the isothermal bands are distorted and the high isothermal band apparently extends to the right upper region.

While the resonant phenomenon occurs, the frequencies of the flow and the vibration are the same. The resonant period of the flow can be considered as the time of the fluid flowing one circle around the enclosure. However, the direction of the acceleration induced by the vibration motion alternates oppositely once during a period; in turn, the direction of the acceleration is the negative y-axis in half a period and the positive y-axis in another half period.

Consequently, the flowing motion of the fluid in the resonant vibration convection region can be described as follows. The fluid first flows from the left lower region; at this time the fluid is hot and the direction of the acceleration is the negative y-axis, then the rotating direction of the flow is clockwise. At the end of the first half period, the fluid must flow to the right upper region (half path of a circle around the enclosure) and the direction of the acceleration will change to the positive y-axis. In order to keep the rotating direction invariant, the fluid must maintain a hot temperature condition in the right upper region to synchronize with the opposite direction of the acceleration.

Based upon the phenomenon mentioned above and the energy equation, the following results can be obtained from the scale analysis method. In the core region

$$T \sim \Delta T = T_h - T_c$$
$$t \sim \Gamma = 2\pi/\Omega$$
$$x, y \sim L$$
$$u, v \sim V^*.$$

Then

$$\frac{\partial T}{\partial t} + \left(u\frac{\partial T}{\partial x} + v\frac{\partial T}{\partial y}\right) = \alpha\left(\frac{\partial^2 T}{\partial x^2} + \frac{\partial^2 T}{\partial x^2}\right)$$

$$\frac{\Delta T}{\Gamma} \qquad \frac{V^*\Delta T}{L} \qquad \frac{\alpha\Delta T}{L^2}$$

$$1 \qquad \frac{V^*\Gamma}{L} \qquad \frac{\alpha\Gamma}{L^2} = \frac{2\alpha\pi}{L^2\Omega} = \frac{2\pi}{\omega}. \tag{12}$$

For the resonant vibration flow, $V^*\Gamma \sim L$, then

$$\frac{V^*\Gamma}{L} \sim 1.$$

Hence, it is suggested that the energy balance occurs mainly between the heat capacity and convection terms at the resonant vibration state. Consequently, the variation of the thermal diffusion term $(2\pi/\omega)$ must be smaller than that of the convection or heat capacity term, and $2\pi/\omega < 1$.

From the viewpoint of dynamics, first consider the y-direction momentum equation inside the Stokes layer δ_v, which is caused by the vibration oscillating flow [29]

$$\frac{dV}{dt} = -\frac{\partial P}{\partial y} + v\frac{\partial^2 v}{\partial x^2} + g\beta\Delta T + b\Omega^2\beta\Delta T\sin\Omega t \tag{13}$$

$$x \sim \delta_v = 4.5\sqrt{(2v/\Omega)}$$
$$y \sim L$$
$$t \sim \pi/\Omega. \tag{14}$$

The magnitudes of the order for the inertia and viscous terms are v/t and vv/x^2, respectively

$$\frac{\text{inertia term}}{\text{viscous term}} \sim \frac{4.5^2 \times 2}{\pi} > 1.$$

The inertia term in the Stokes layer is larger than the viscous term. The following equation can be determined:

inertia term ~ buoyancy term

$$\frac{dv}{dt} \sim b\Omega^2\beta\Delta T\sin\Omega t + g\beta\Delta T. \tag{15}$$

The resonant phenomenon is caused by the oscil-

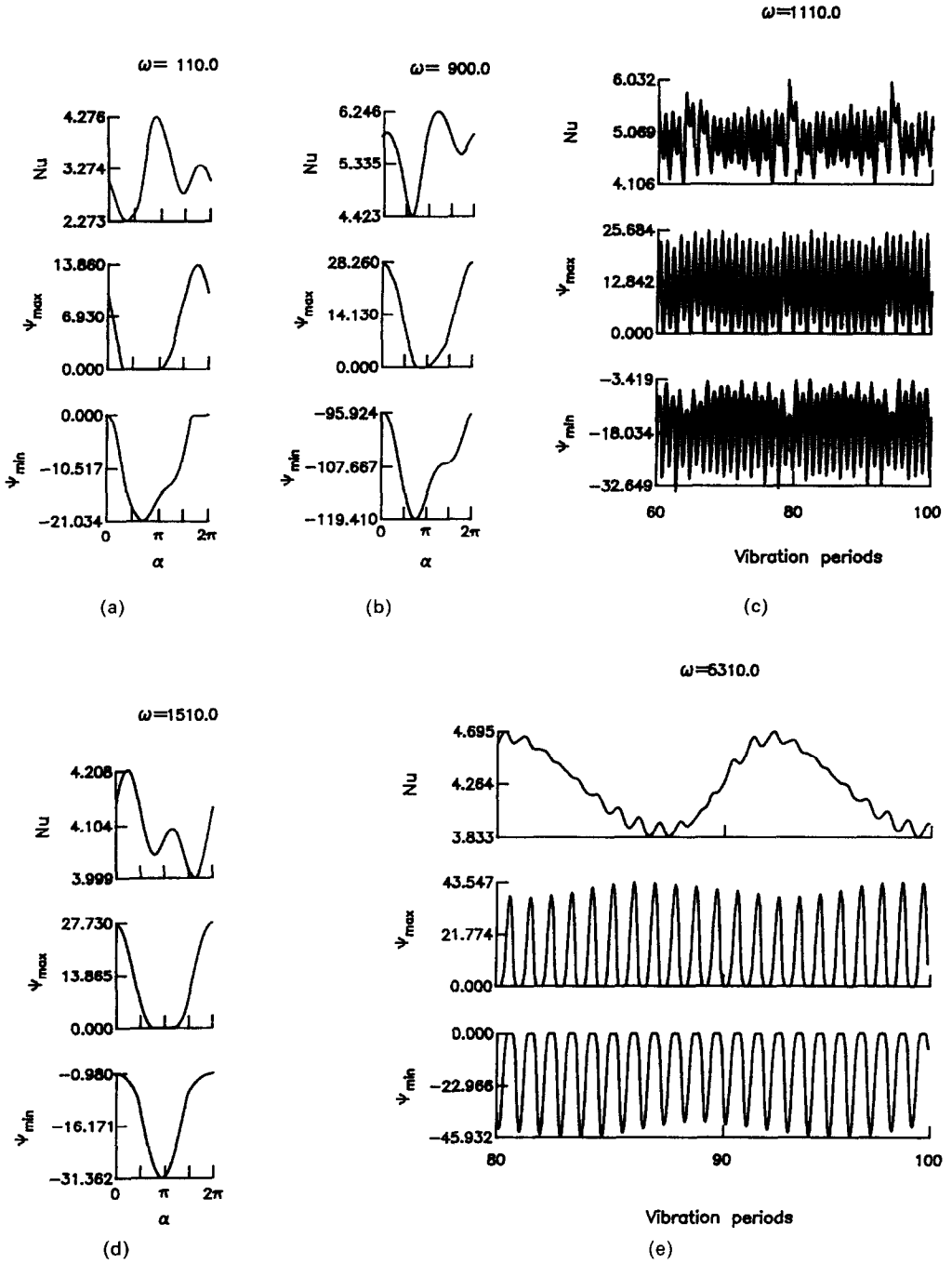

FIG. 15. The variations of the Nusselt number, the maximum and minimum values of stream function with the vibration phase angle (α) for $Ra = 10^4$, $G = 10^6$. (a) $\omega = 110$, (b) $\omega = 900$, (c) $\omega = 1110$, (d) $\omega = 1510$, (e) $\omega = 5310$.

lating flow induced by the vibration, and the static gravity somewhat affects the resonant frequency. Therefore, equation (15) can be expressed as

$$\frac{dv}{dt} \sim b\Omega^2\beta\Delta T \sin \Omega t \tag{16}$$

$$v \sim b\Omega\beta\Delta T \cos \Omega t. \tag{17}$$

At resonant state, the flow frequency is equal to the vibration frequency; thus the following equation is determined:

$$4L = \int_0^{2\pi/\Omega_r} |v|\, dt. \tag{18}$$

Substituting equation (17) into equation (18) and solving the resonant frequency Ω_r

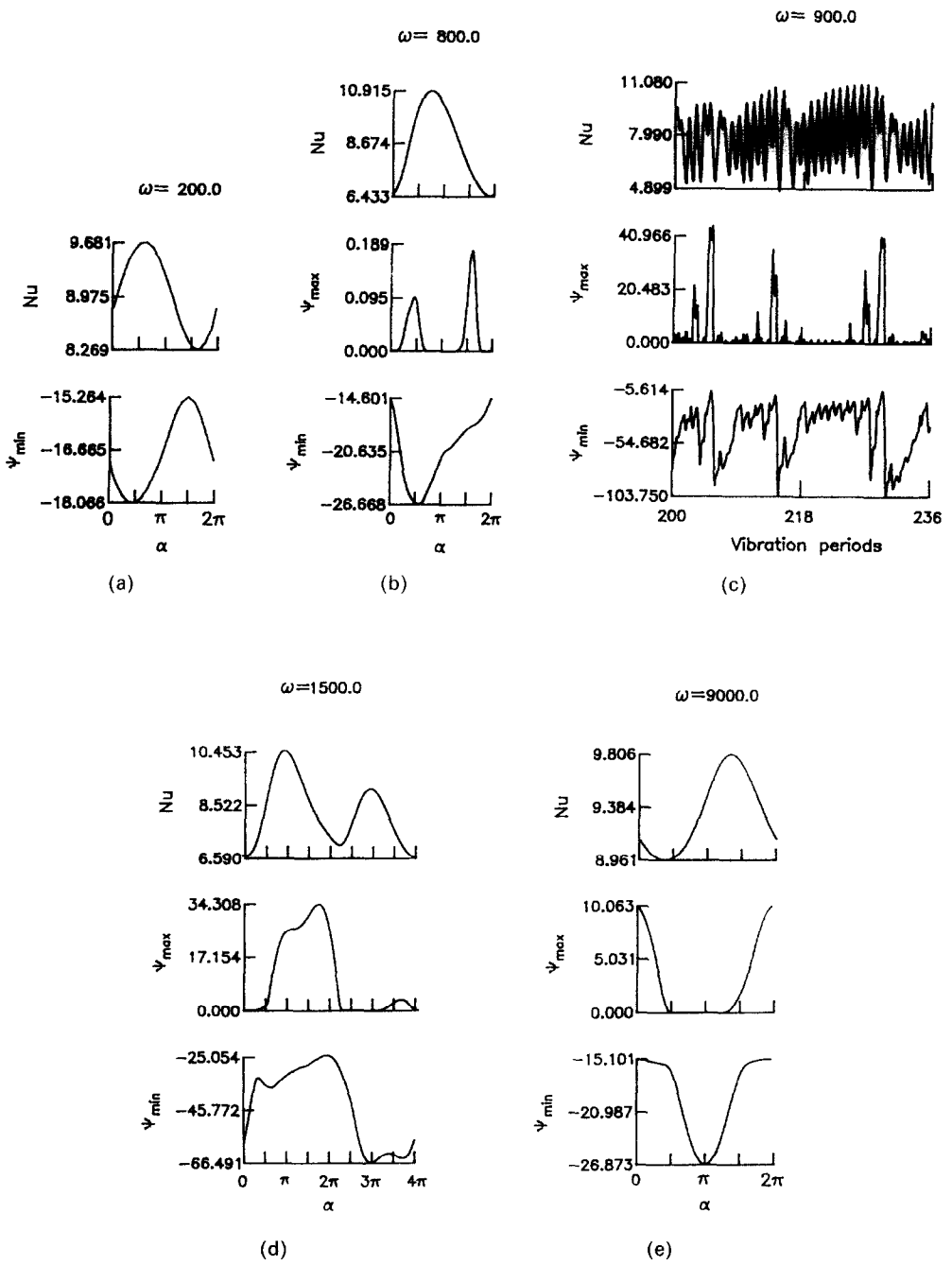

FIG. 16. The variations of the Nusselt number, the maximum and minimum values of stream function with the vibration phase angle (α) for $Ra = 10^6$, $G = 10^6$. (a) $\omega = 200$, (b) $\omega = 800$, (c) $\omega = 900$, (d) $\omega = 1500$, (e) $\omega = 9000$.

$$L = b\beta\Delta T \tag{19}$$

$$\omega_r = \sqrt{(2G)}\,Pr \tag{20}$$

in which $\omega_r = \Omega_r L^2/\alpha$.

Solving equation (20), the value of the resonant frequency ω_r for the $G = 10^6$, $Pr = 0.71$ case is about 1000, which is in agreement with those values obtained from the numerical method in this study. In Table 2,

Table 2. Comparisons of the resonant frequency proposed by the authors ($\sqrt{(2G)\cdot Pr}$) with those of Yurkov [20] ($Pr = 1$)

G	Data from ref. [20]	$\sqrt{(2G)\cdot Pr}$
9×10^4	272	424
1.6×10^5	558	565
2.5×10^5	722	707
3.6×10^5	890	848

the solutions obtained from equation (20) are compared with those of Yurkov [20] (from Fig. 14 of ref. [7]). The deviations between both solutions are allowable except for the $G = 9 \times 10^4$ case.

CONCLUSIONS

The study of thermal convection in a two-dimensional square enclosure induced simultaneously by gravity and vibration is investigated by a penalty finite element method. Several conclusions can be drawn.

(1) According to the individual characteristic, the thermal convection can be divided into five regions: (i) quasi-static convection; (ii) vibration convection; (iii) resonant vibration convection; (iv) intermediate convection; and (v) high frequency vibration convection.

(2) In the high Rayleigh number case ($Ra = 10^6$), the gravitational thermal convection dominates, and the vibration does not enhance the heat transfer rate remarkably. In contrast, in the low Rayleigh number case ($Ra = 10^4$), except in the quasi-static convection region, the vibration thermal convection is dominant, and the vibration enhances the heat transfer rate significantly.

(3) According to Fu and Shieh [24], the quasi-static convection region can be determined approximately by the following relation:

$$\omega = Pr^{1/2}\, Ra^{3/4}(2G)^{-1/4}.$$

(4) The resonant frequency ω_r derived from the preliminary estimation can be expressed as $\omega = \sqrt{(2G)} \cdot Pr$. The results predicted by the equation are in agreement with those obtained from numerical methods.

Acknowledgement—The support of this work by the national Science Council, Taiwan, R.O.C. under contract NSC79-0401-E-009-10 is gratefully acknowledged.

REFERENCES

1. S. Ostrach, Natural convection in enclosures, *Adv. Heat Transfer* **8,** 161–227 (1972).
2. S. Ostrach, Natural convection heat transfer in cavities and cells, *Heat Transfer* **1,** 365–379 (1982).
3. S. Ostrach, Natural convection in enclosures, *J. Heat Transfer* **110,** 1175–1189 (1988).
4. I. Catton, Natural convection in enclosures, *Heat Transfer* **6,** 13–43 (1978).
5. K. T. Yang, Natural convection in enclosures. In *Handbook of Single Phase Convective Heat Transfer*, pp. 13.1–13.51. Wiley-Interscience, New York (1987).
6. P. D. Richardson, Effects of sound and vibrations on heat transfer, *Appl. Mech. Rev.* **20,** 201–217 (1967).
7. G. Z. Gershuni and E. M. Zhukhovitsky, Vibrational thermal convection in zero gravity, *Fluid Mech.—Sov. Res.* **15,** 63–84 (1986).
8. R. E. Forbes, C. T. Carley and C. J. Bell, Vibration effects on convective heat transfer in enclosures, *J. Heat Transfer* **92,** 429–438 (1970).
9. A. A. Ivanova and V. G. Kozlov, Vibrationally gravitational convection in a horizontal cylindrical layer, *Heat Transfer—Sov. Res.* **20,** 235–247 (1988).
10. A. A. Ivanova, Influence of vibrations of the unsteady-state convective heat transfer in a cylindrical cavity, *Heat Transfer—Sov. Res.* **20,** 248–251 (1988).
11. M. P. Zavarykin, S. V. Zorin and G. F. Putin, Experimental study of vibrational convection, *Dokl. Akad. Nauk SSSR* **281,** 815–816 (1985).
12. M. P. Zavarykin, S. V. Zorin and G. F. Putin, Convective instabilities in a vibrational field, *Dokl. Akad. Nauk SSSR* **299,** 309–312 (1988).
13. G. Z. Gershuni and E. M. Zhukhovitskii, On parametric excitation of convective instability, *Prikl. Mat. Mekh.* **27,** 779–783 (1963).
14. G. Z. Gershuni, E. M. Zhukhovitskii and Yu. S. Yurkov, On convective stability in the presence of periodically varying parameter, *Prikl. Mat. Mekh.* **34,** 470–480 (1970).
15. S. M. Zenkovskaya and I. B. Simonenko, Effect of high frequency vibration on convection initiation, *Izv. AN SSSR, Mech. Zhidk. Gaza* **1**(5), 51–55 (1966).
16. G. Z. Gershuni, E. M. Zhukhovitskii and Yu. S. Yurkov, Vibrational thermal convection in a rectangular cavity, *Izv. AN SSSR, Mech. Zhidk. Gaza* No. 4, 94–99 (1982).
17. A. N. Sharifulin, Supercritical vibration-induced thermal convection in a cylindrical cavity, *Fluid Mech.—Sov. Res.* **15**(2), 335–338 (1986).
18. R. R. Siraev, Vibrational thermal convection about a uniformly heated cylinder, *Izv. AN SSSR, Mekh. Zhidk. Gaza* No. 3, 23–26 (1989).
19. Yu. S. Yurkov, Vibration-induced thermal convection in a square cavity in weightlessness at arbitrary frequencies. In *II Vsesoyuznyye seminor po gidromekhanike i teplomassoobmenu V nevesomosti* [Tezisy dokladov], Perm, pp. 36–37 (1981). (Reviewed in ref. [7].)
20. Yu. S. Yurkov, Vibration-induced thermal convection in a square cavity in weightlessness (finite frequencies). In *Konvektivnyye techeniya*, Convective Perm Teachers' Institute, Perm, pp. 98–103 (1981). (Reviewed in ref. [7].)
21. S. Biringen and G. Danabasoglu, Computation of convective flow with gravity modulation in rectangular cavities, *J. Thermophys.* **4,** 357–365 (1990).
22. P. M. Gresho and R. L. Sani, The effects of gravity modulation on the stability of a heated fluid layer, *J. Fluid Mech.* **40,** 783–806 (1970).
23. S. Biringen and L. J. Peltier, Numerical simulation of 3-D Benard convection with gravitational modulation, *Physics Fluids* **A2,** 754–764 (1990).
24. W. S. Fu and W. J. Shieh, A numerical study of transient natural convection under time-dependent gravitational acceleration field, *Wärme- und Stoffübertragung* **27,** 109–117 (1992).
25. R. J. Schoenhals and J. A. Clar, Laminar free convection boundary-layer perturbations due to transverse wall vibration, *J. Heat Transfer* **84,** 225–234 (1962).
26. W. S. Fu, J. C. Perng and W. J. Shieh, Transient laminar natural convection in an enclosure partitioned by an adiabatic baffle, *Numer. Heat Transfer* **16A,** 325–359 (1989).
27. G. De Vahl Davis, Natural convection of air in a square cavity: a bench mark numerical solution, *Int. J. Numer. Meth. Fluids* **3,** 249–264 (1983).
28. A. H. Nayfeh, *Nonlinear Oscillation*, Chap. 4, p. 161. Wiley, New York (1979).
29. R. L. Panton, *Incompressible Flow*, Chap. 11, p. 266. Wiley, New York (1984).

ETUDE DE LA CONVECTION THERMIQUE DANS UNE CAVITE INDUITE SIMULTANEMENT PAR GRAVITE ET VIBRATION

Résumé—On étudie numériquement la convection thermique dans une cavité bidimensionnelle carrée, en présence de gravité et d'une vibration verticale. Une méthode d'éléments finis avec un algorithme d'itération Newton–Raphson et un schéma de différences rétrograde avec le temps sont adoptés pour résoudre les équations. Pour étudier les effets de la fréquence de vibration et du nombre de Rayleigh sur la convection thermique, la fréquence varie entre 1 et 10^4 et on considère trois valeurs différentes du nombre de Rayleigh soit 0, 10^4 et 10^6. D'après les résultats, la convection thermique peut être divisée en cinq régions: (1) convection quasi-statique, (2) convection de vibration, (3) convection de vibration résonante, (4) convection intermédiaire et (5) convection de vibration à haute fréquence. Au nombre de Rayleigh élevé ($=10^6$), la convection thermique gravitationnelle domine et le mouvement de vibration n'augmente pas sensiblement le flux de chaleur transféré. Par contre, au faible nombre de Rayleigh, ($=10^4$), excepté dans la région de convection quasi-statique, la convection thermique de vibration est dominante et la vibration augmente significativement le transfert de chaleur. De plus, on propose deux méthodes analytiques pour prédire les fréquences de la convection quasi-statique et les régions de convection de vibration résonante. Les valeurs prédites par les deux méthodes sont en accord avec celles obtenues par la méthode numérique.

UNTERSUCHUNG DER DURCH SCHWERKRAFT UND VIBRATION INDUZIERTEN THERMISCHEN KONVEKTION IN EINEM HOHLRAUM

Zusammenfassung—Die durch die gleichzeitige Einwirkung von Schwerkraft und vertikaler Vibration in einem zweidimensionalen quadratischen Hohlraum induzierte thermische Konvektion wird numerisch untersucht. Eine Finite-Elemente-Methode mit einem Newton–Raphson-Iterations-Algorithmus und ein Rückwärtsdifferenzen-Verfahren für den Zeitterm werden bei der Lösung der bestimmenden Gleichungen verwendet. Um den Einfluß von Vibrationsfrequenz und Rayleigh-Zahl auf die Konvektion zu untersuchen, wird die Frequenz von 1 bis 10^4 bei Rayleigh-Zahlen von 0, 10^4 und 10^6 variiert. Es zeigt sich, daß die thermische Konvektion in fünf Bereiche aufgeteilt werden kann: (i) quasi-statische, (ii) Vibrations-, (iii) Resonanz-Vibrations-, (iv) intermediäre und (v) Hochfrequenz-Vibrations-Konvektion. Bei großer Rayleigh-Zahl (10^6) dominiert die Gravitations-Konvektion, und die Vibrationen erhöhen den Wärmeübergang nicht merklich. Im Bereich 10^4 dagegen (ausgenommen im quasi-statischen Konvektions-Bereich) dominiert die Vibrations-Konvektion, und der Wärmeübergang wird deutlich verbessert. Weiterhin werden zwei analytische Methoden vorgeschlagen, mit denen die Frequenzen der quasi-statischen Konvektion, bzw. der Gebiete mit Resonanz-Vibrations-Konvektion berechnet werden können. Die hierbei ermittelten Werte stimmen mit den nach der numerischen Methode bestimmten überein.

ИССЛЕДОВАНИЕ ТЕПЛОВОЙ КОНВЕКЦИИ В ПОЛОСТИ ЗА СЧЕТ СИЛЫ ТЯЖЕСТИ И ВИБРАЦИИ

Аннотация—Численно исследуется тепловая конвекция в двумерной квадратной полости за счет совместного действия силы тяжести и вертикальной вибрации. Для решения определяющих уравнений используются метод конечных элементов с итерационным алгоритмом Ньютона–Рэфсона и обратная разностная схема, учитывающая временные члены. Для установления влияния частоты вибрации и числа Рэлея на тепловую конвекцию в полости частота вибраций варьируется от 1 до 10^4 и рассматриваются три различных значения числа Рэлея, равные 0, 10^4 и 10^6. В соответствии с полученными результатами тепловую конвекцию можно разделить на пять областей: (I) квазистатическая конвекция, (II) виброконвекция, (III) резонансная виброконвекция, (IV) промежуточная конвекция и (V) высокочастотная виброконвекция. В случае высокого числа Рэлея (10^6) преобладает гравитационная тепловая конвекция и вибрационное движение не приводит к значительной интенсификации теплопереноса. В случае же низкого числа Рэлея (10^4) всюду за исключением области квазистатической конвекции доминирует вибрационная тепловая конвекция и вибрационное движение существенно увеличивает скорость теплопереноса. Кроме того, предложены два аналитических метода расчета частот для областей квазитатической конвекции и резонансной виброконвекции. Значения, полученные при расчетах с использованием этих методов, согласуются с численными результатами.